Computers and Concrete, Vol. 2, No. 3 (2005) 215-238
DOI: http://dx.doi.org/10.12989/cac.2005.2.3.215

Numerical investigation of RC structural walls subjected to cyclic loading

D. M. Cotsovos†

Concept Engineering Consultants, London W3 0RF, UK

M. N. Pavlović‡

Department of Civil & Environmental Engineering, Imperial College, London SW7 2AZ, UK

(Received June 26, 2004, Accepted May 25, 2005)

Abstract This work is based on a nonlinear finite-element model with proven capacity for yielding realistic predictions of the response of reinforced-concrete structures under static monotonically-increasing loading. In it, the material description relies essentially on the two key properties of triaxiality and brittleness and, thus, is simpler than those of most other material models in use. In this article, the finite-element program is successfully used in investigating the behaviour of a series of RC walls under static cyclic loading. This type of loading offers a more strenuous test of the validity of the proposed program since cracks continuously form and close during each load cycle. Such a test is considered to be essential before attempting to use the program for the analysis of concrete structures under seismic excitation in order to ensure that the solution procedure adopted is numerically stable and can accurately predict the behaviour of RC structures under such earthquake-loading conditions. This is achieved through a comparative study between the numerical predictions obtained presently from the program and available experimental data.

Keywords: concrete; nonlinear analysis; RC walls; finite elements; cyclic loading.

1. Introduction

Over the past decades a number of finite-element (FE) packages have been produced, with the aim to accurately predict the behavior of reinforced-concrete (RC) structures under static and dynamic loading. A large number of material models have been incorporated into such packages in order to describe the nonlinear behaviour of concrete. Their formulations has been based on a variety of theories such as plasticity (Murray, *et al.* 1979, Chen and Chen 1975, Yasuhiro and Chen 1987, Kang, *et al.* 2000, Grassl, *et al.* 2001), viscoplasticity (Chen 1988, Cela 1998, Winnicki, *et al.* 2001), continuum damage mechanics (Mazars 1986, Papa and Taliercio 1996, Hatzigeorgiou, *et al.* 2001, Baluch, *et al.* 2003, Al-Gadhib, *et al.* 1998, 2000) or a combination of these theories (Fardis, *et al.* 1983, Chen and Buyukozturk 1985, Yang, *et al.* 1985, Dube, *et al.* 1996, Winnicki and Cichon 1998a,b, Faria, *et al.* 1998). Such models are usually referred to as phenomenological since they are based on theories capable of providing a close fit to experimental information without

† Principal Engineer
‡ Head of Concrete Structures, m.pavlovic@ic.ac.uk

taking into consideration the causes of the observed material behaviour. Regardless of the theory upon which their formulation is based, these models share a number of fundamental assumptions, the validity of which is inherently questioned in the present work. Strain softening and stress-path dependency are the most common among such assumptions. In order for such material models to be used in certain problems, one must initially calibrate (based on available experimental data) them carefully by assigning certain values to a number of parameters which are essential in order to fully define the material model. However, the use of such parameters usually makes the FE packages which incorporate them case-sensitive due to the fact that their ability to produce accurate predictions is limited only to certain types of problems. Applying them to different problem types often means that they have to be recalibrated.

In contrast to the vast majority of FE packages produced to date, the present work is based on a nonlinear FE program which incorporates a brittle model of concrete behaviour, which has been shown to be capable of yielding realistic predictions of the response of a wide range of RC structures under static monotonically-increasing loads (Kotsovos and Pavlović 1995). The same program was later modified in order to account for crack closure (Kotsovos and Spiliopoulos 1998). This material model does not account for strain softening nor stress-path dependency, but places special emphasis on the response of concrete to multiaxial stress conditions.

Imposing a cyclic load to an RC structure causes the formation and closure of a number of cracks during each load reversal. Such crack formation and closure may also occur under monotonic loading conditions - but on a much smaller scale, and hence crack reversal under such circumstances can usually be ignored for purposes of estimating the collapse load (Kotsovos and Spiliopoulos 1998). However, under static cyclic loading this is not the case, especially in cases where the level of loading approaches the load-carrying capacity of the structural form under investigation. The cracking procedure that the RC structure undergoes during each load cycle leads to a gradual degradation of the concrete medium which may ultimately affect its load-carrying capacity. Therefore, the case of cyclic loading offers a more strenuous test of the validity of the proposed program and of its ability to accurately model the crack opening and closure procedure that the concrete medium undergoes during the application of each load cycle. As Kwak and Kim (2004) rightly point out "[whereas] many experimental and analytical studies for predicting the nonlinear behavior according to load reversals…of…shear walls have been performed…in contrast, numerical models for FE analyses of RC shear walls, which can provide accurate simulations of cracking behaviour under severe cyclic conditions…are somewhat less commonly used due to the complexities in the hysteretic modeling…after cracking or crushing of concrete and yielding of steel" (pp 77-78). Such a "strenuous test" is considered to be essential before attempting to use the program for the analysis of RC structures under dynamic loading. The present work reports one such series of numerical tests, in which the response of a number of RC walls (for which experimental data is available) is investigated under static cyclic loading. The comparative study will prove that the proposed FE program is numerically stable and can produce accurate predictions for the behaviour of RC structures under such loading.

2. Material modelling

Based on experimental data initially presented by Kotsovos (1983) and later by Van Mier (1984) and Zissopoulos, *et al.* (2000), it is clear that the descending branch does not describe material

behaviour but is the result of interaction between specimen and testing device. This implies that concrete is essentially a brittle material, a view which has recently gained wide acceptance among material specialists – as evidenced in the findings of the report by the relevant RILEM technical committee (Van Mier, *et al.* 1997) – but has failed to be implemented by the majority of FE analysts working in the field of nonlinear modelling of concrete. Furthermore, the experimental data upon which the analytical formulation of all concrete constitutive models (published to date) is based is characterized by a significant scatter. Even when using valid experimental data, this scatter is still substantial. Experimental results (Kotsovos 1979) reveal that any stress-path dependency in concrete behaviour disappears within the scatter of the experimental results. Hence, any effect attributed to stress-path dependency cannot be quantified and it is both realistic and, for practical purposes, accurate to consider that concrete behaviour is stress-path independent.

In view of the above, the present work adopts a three-dimensional (3D) material model for concrete which is both brittle and independent of stress-path effects. Its formulation was derived from an analysis of experimental data, the validity of which was verified during an international cooperative project investigating the effect of testing techniques on concrete behaviour under triaxial stress conditions (Kotsovos and Pavlović 1995). The brittle nature of the model bypasses the need to introduce extra material parameters associated with the strain-softening assumption. Self-evidently, stress-path independency also results in a radical simplification to many of the material models used hitherto. Thus, the proposed concrete model offers considerable advantages in FE analysis.

In order for a material model of concrete behaviour to be successfully used in problems where the loading history consists of load cycles, such a model must be able to describe the hysteretic behaviour of concrete. Presently, the assumption is made that during unloading the behaviour of concrete resembles that of a linear material, as depicted in Fig. 1. At some point in the loading procedure, the load is gradually decreased to a certain level and then it is gradually increased again

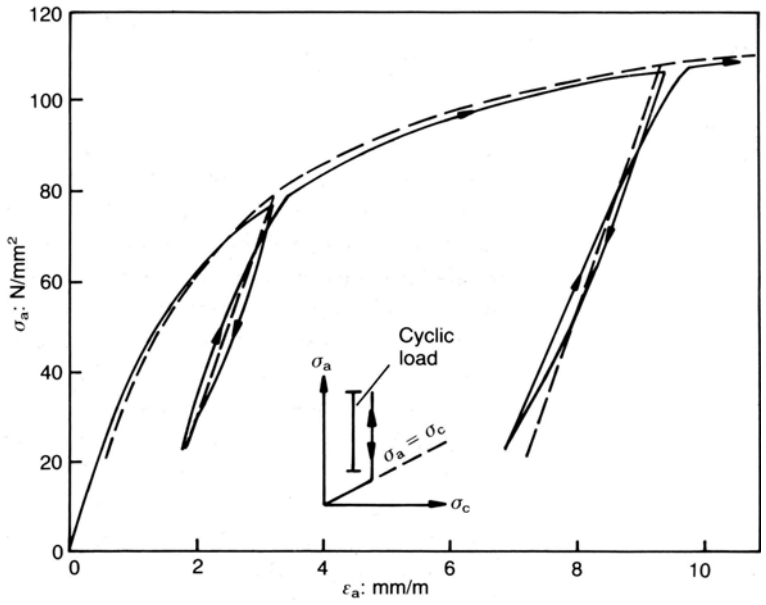

Fig. 1 Behavior of concrete during loading-unloading-reloading

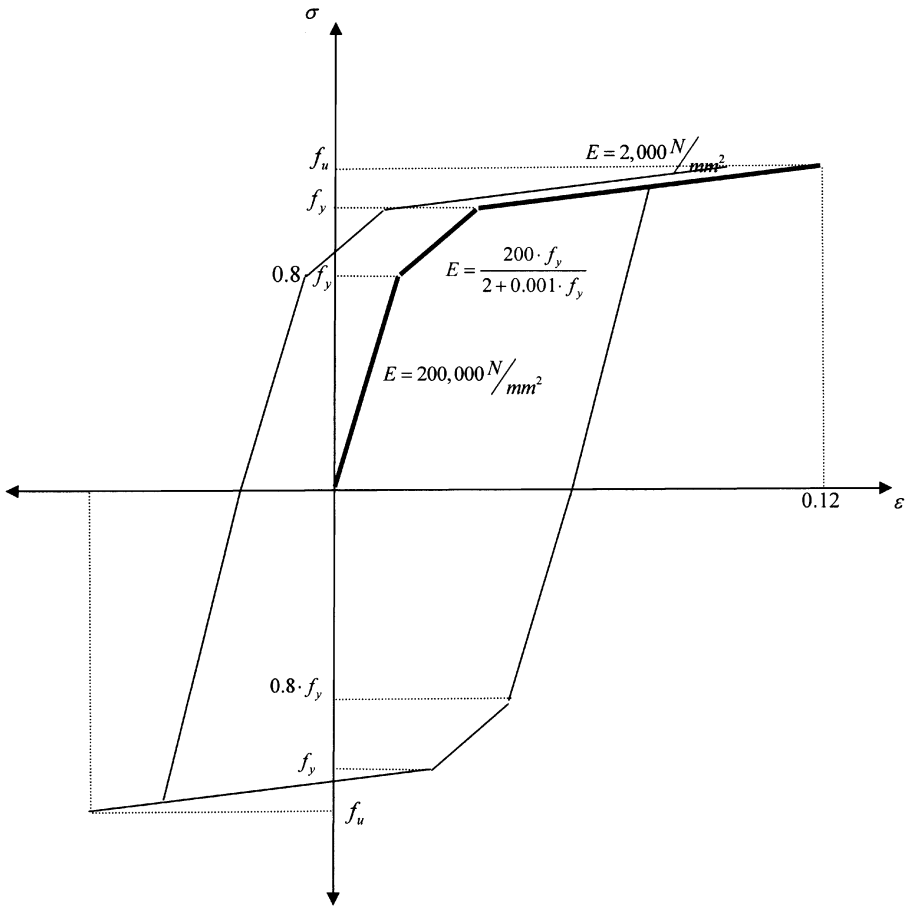

Fig. 2 Constitutive model for the steel reinforcement

(loading – unloading – reloading), thus causing the stress-strain curve to form a hysteretic loop. It is interesting to note in Fig. 1 that the area enclosed by the loop is small. Based on this observation, it can be assumed that the behaviour of concrete during unloading/reloading may be realistically described by a simple linear model based on Hooke's law using elastic material properties.

Under monotonically applied load, the constitutive model used to describe the behaviour of steel reinforcement under uniaxial tension and compression is a simple tri-linear model (Fig. 2a). It is divided into three linear sections. In each one of these sections, the material properties remain constant. However, when moving from one section onto another (with increasing stress) the material properties change resulting in an abrupt reduction of the stiffness. The first and second sections of the stress-strain diagram are defined by the yield stress (Fig. 2a). The third section starts from the point where the stress is equal to the yield stress f_y and has a very small inclination, usually 1% of the slope of the first elastic section. As a result, small increases in stress cause large increases in strain. The steel-reinforcement fails when the strain attains its ultimate value $\varepsilon_u(\varepsilon_u = 0.12)$ or when the stress reaches the value of the ultimate stress (f_u). Under load reversals the stress-strain relations which describe the behaviour of the steel reinforcement bars when subjected to uniaxial tension or compression is presented graphically in Fig. 2.

3. Nonlinear FE solution procedure

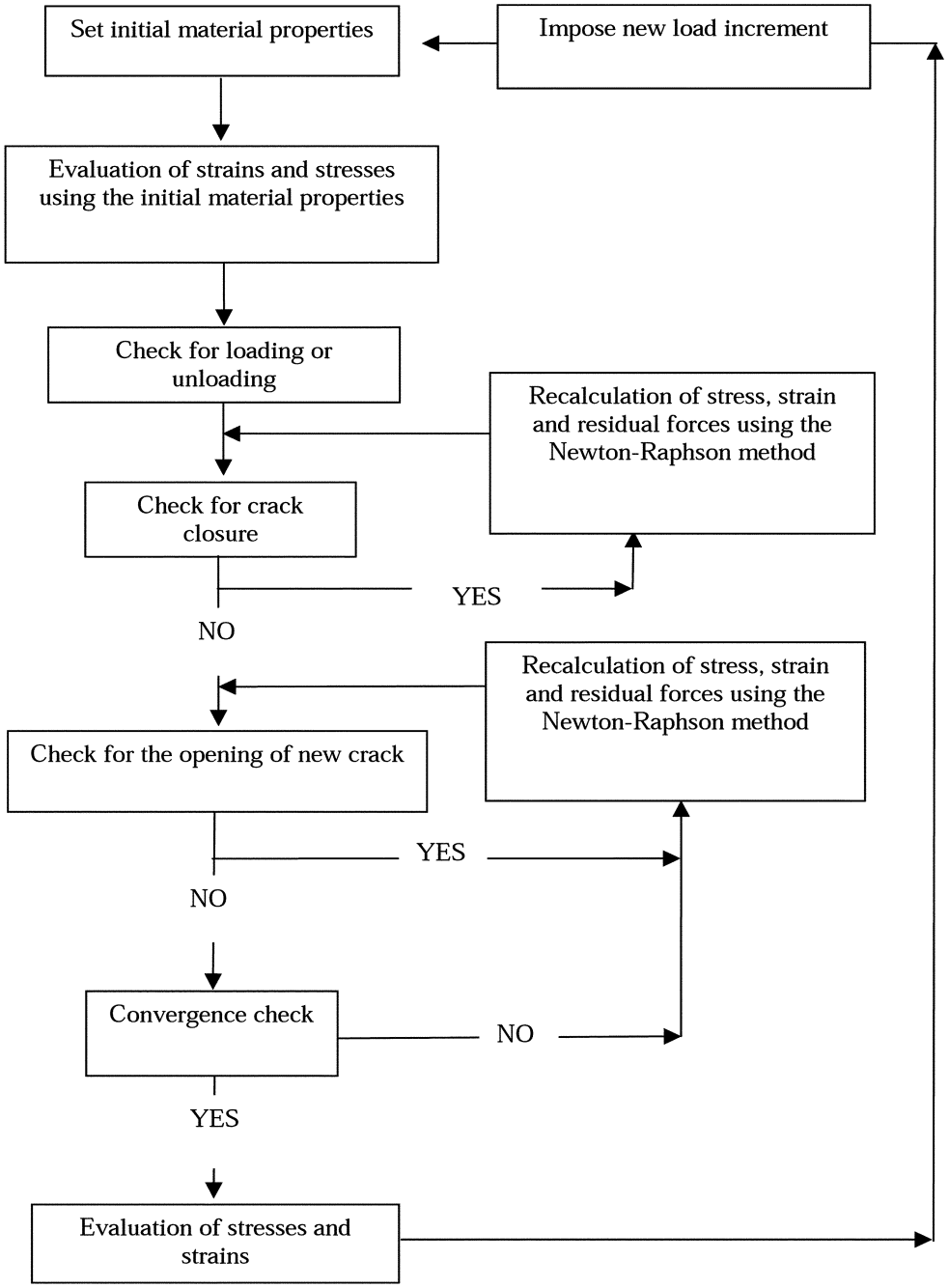

Fig. 3 Scheme of the used by the nonlinear FE program

The proposed FE model uses 3D analysis, employing the 3D material model to account for the triaxial behaviour of concrete and 27-node Lagrangian isoparametric brick elements for the modelling of the concrete medium. The need for 3D analysis is dictated by the non-homogeneous nature of concrete as a material and the cracking procedure it undergoes when subjected to an external load which, in turn, results in the formation of a complex spatial stress field within the concrete medium which continuously changes due to the redistribution of stresses caused by the ongoing cracking preceded by unavoidable triaxiality (Kotsovos and Pavlović 1995).

Due to the nonlinear behaviour of the material, the nonlinear analysis is based on an iterative procedure, known as the modified Newton-Raphson method (Kotsovos and Pavlović 1995) which is used in order to calculate stresses, strains and the residual forces. Once the load increment is imposed, the iterative procedure commences. At first, every Gauss point is checked in order to determine whether loading or unloading is taking place. Then, a number of checks are carried out to establish whether any cracks close or open, or if any steel members yield or even fail. Depending on the results of the previous checks, changes are introduced to the stress-strain matrices of the individual FE's and, consequently, to the stiffness matrix of the structure. Based on these modified matrices, deformation, strain and stress corrections are evaluated. Convergence is accomplished once the above corrections become very small. At this point it should be pointed out that the formation and closure of cracking is checked separately during each load step. The nonlinear iterative procedure adopted by the program is presented in Fig. 3 (Kotsovos and Pavlović 1995, Kotsovos and Spiliopoulos 1998).

During the crack-closure procedure only Gauss points with cracks formed in previous load steps are checked. For a crack to close, the criterion that must be satisfied is that the strains normal to the plane of the crack are compressive. The program singles out the crack with the largest compressive strain and closes it. Because of the closure of a crack, changes need to be made to the element stress-strain matrix and, consequently, to the stiffness matrix of the structure, leading to redistribution of the stresses inside the structure. At this point it should be pointed out that, during the crack-closing procedure, convergence is not checked. This means that the residual stresses and forces are not eliminated during this stage of the iterative procedure but are only calculated and added to those calculated in previous iterations. During each iteration, only one crack may close (the crack with the largest value of compressive strain normal to its plane). It has been observed that, after the closure of one crack, there is a drastic drop in the number of cracks that need to close next. The crack-closing procedure is repeated until all cracks that fulfill the crack-closure criterion close.

After the crack-closure procedure is completed, the crack-opening procedure commences. During each iteration of this procedure all Gauss points are checked in order to determine if any new cracks form. This is achieved by using the failure criterion since the opening of a crack corresponds to localized failure of the material. The formation of a crack leads to the modification of the element stress-strain matrix and the stiffness matrix of the structure, thus causing redistribution of the internal stresses. In order to avoid numerical instabilities during the solution of the problem, only a limited number of cracks (no more than three) are allowed to form per iteration. Should the number of cracks that need to open exceed this predefined number, then only the most critical cracks will be allowed to form. The most critical cracks are those which correspond to the Gauss points with the largest values of tensile stress and strain acting normal to the plane of the crack. Usually, after the formation of the most critical cracks the number of cracks that need to form in the next iteration reduces rapidly due to the redistribution of stress achieved during this process. Unlike the crack-

closure procedure, convergence of the residual forces is now checked after all cracks have opened. If the maximum value of the residual forces evaluated is greater than a certain predefined value, then these residual forces are re-imposed onto the structure in the form of an external loading.

Crack formation is modelled by using the smeared-crack approach. A crack forms when the stress developing in a given part of the structure corresponds to a point in the principal stress space that lies outside the surface defining the failure criterion for concrete, thus resulting in localized material failure. This failure takes the form of a crack. The plane of the crack is normal to the direction in which the smallest principal stress acts (largest tensile stress). Failure is followed by immediate loss of load-carrying capacity in the direction normal to the plane of the crack. Concurrently, the shear stiffness is also considered to reduce drastically to a small percentage of its previous value (during the uncracked state). However, it is not set to zero in order to minimize the risk of numerical instabilities during the execution of the solution procedure. Perfect bond between concrete and steel is assumed.

4. Structural walls – summary of the original experimental investigation

The structures investigated are three RC structural walls (specimens SW31, SW32 and SW33), taken from the set of experiments conducted by Lefas (1988). All walls were 650 mm wide, 1300 mm high and 70 mm thick. The values of the uniaxial cylinder compressive strength (f_c) of the concrete used for the walls are given in Table 1, whereas the yield stress (f_y) and ultimate strength (f_u) of the reinforcement appear in Table 2. An identical arrangement of reinforcement was used for all three specimens and this is shown in Fig. 4. During the experiment each wall was monolithically connected to a rigid RC prism at both top and bottom. The bottom prism was firmly bolted to the laboratory strong floor in order to resemble a rigid type of foundation, while at the end faces of the top prism the external loading was imposed through two 50-ton jacks. The prisms were designed so as to remain undamaged throughout the course of the experiment. Each wall was subjected to different cyclic loading conditions. After a prescribed number of load cycles, the load increased monotonically up to the full loss of load-carrying capacity. The loading histories used for the tests are presented in Fig. 5. On the right-hand side, the loading history is presented in the form of imposed displacements, whereas, on the left-hand side, it is presented in the form of imposed forces.

Table 1 Compressive strength of concrete

Specimen	Uniaxial compressive strength f_c (MPa)
SW31	35.2
SW32	53.6
SW33	49.2

Table 2 Yield stress and strength of steel reinforcement

Bar diameter (mm)	Yield strength f_y (MPa)	Ultimate strength f_u (MPa)
8	470	560
6.25	520	610
4	420	480

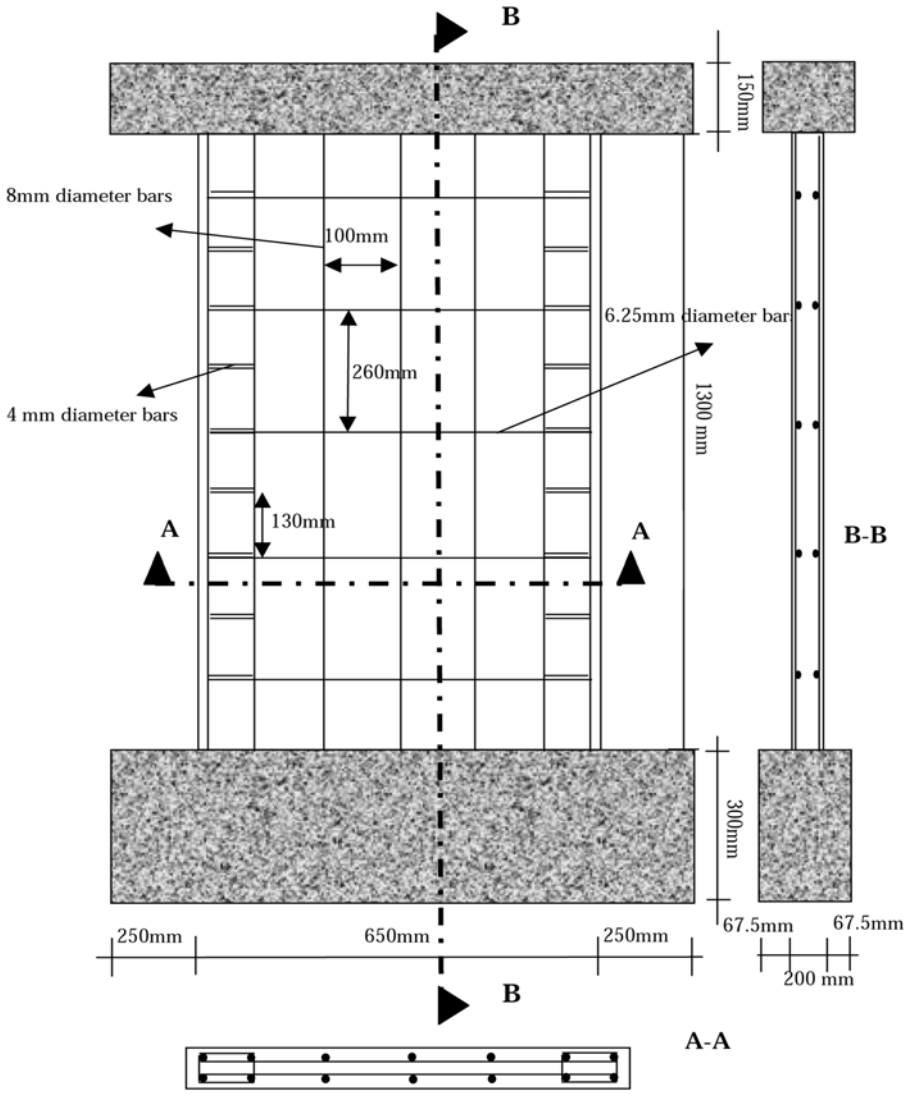

Fig. 4 Arrangement of the reinforcement for the RC walls tested

The results obtained from the experiments are presented in Fig. 6 in the form of load–displacement curves. These figures represent the relations between external load and horizontal displacement at the top of the wall. It can be seen that the maximum value of the cyclic load differs from experiment to experiment. For the case of specimen SW31 (subjected to four load cycles, followed by monotonic loading to failure), the maximum value of the cyclic load was 60% of the load-carrying capacity of the specimen when the load eventually increased to failure, whereas in the case of specimen SW32 (subjected to the same loading pattern as SW31) it was 90%. On the other hand, for specimen SW33 the cyclic loading had a maximum value of 60% of the specimen's load-carrying capacity for the first two loading cycles, which was then increased to 90% for the next two cycles, and finally to (by definition) 100% for the final loading cycle (i.e. fifth cycle) after which

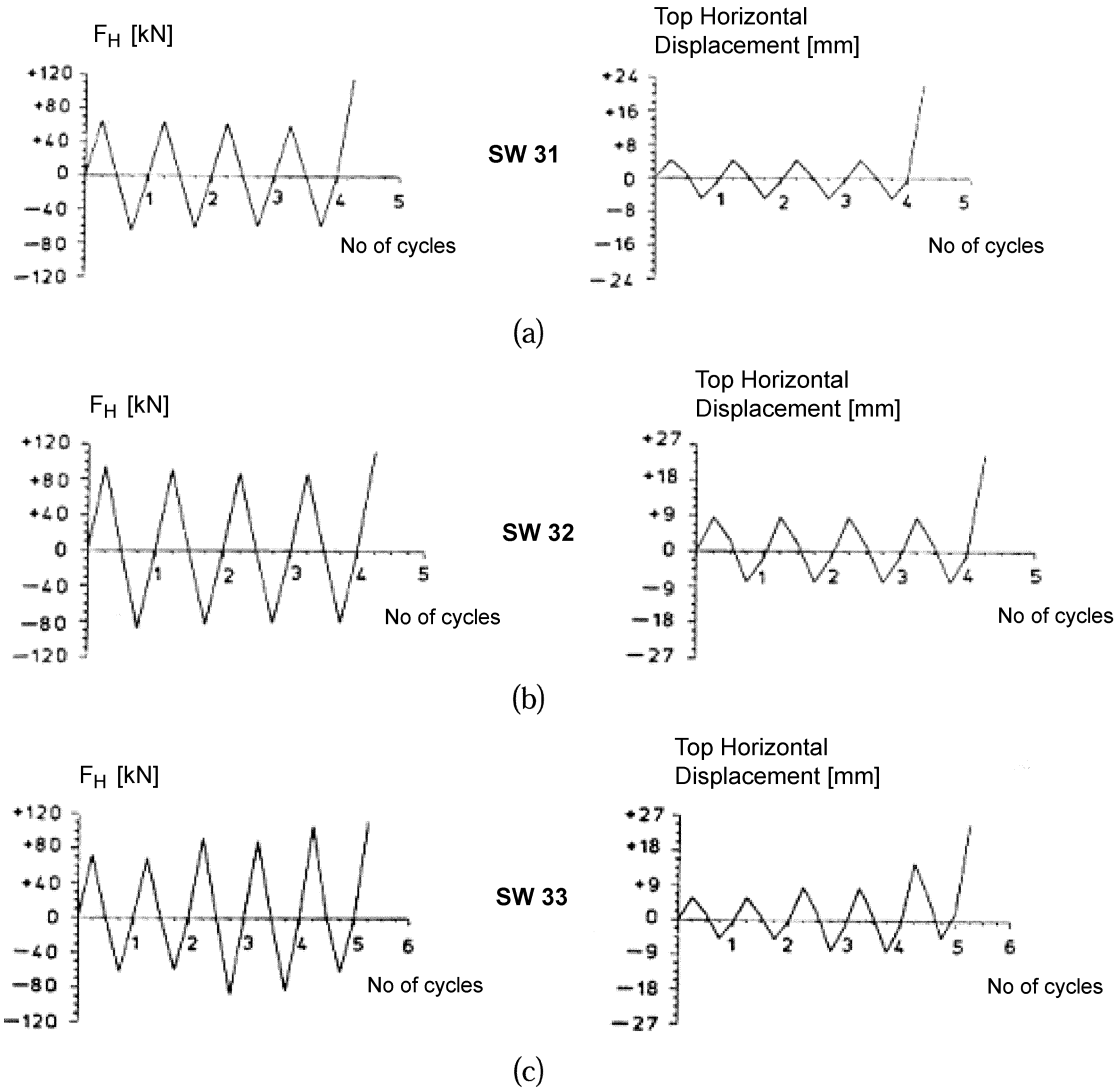

Fig. 5 Load history imposed on specimens: (a) SW31, (b) SW32 and (c) SW33

SW33 was subjected to a further (but monotonic) loading to failure.

5. FE modelling of the RC walls

Concrete is modelled by using 27-node Lagrangian brick elements whereas 3-node isoparametric truss elements are used for the modelling of the reinforcement. The structural walls discussed above were discretizied as shown in Fig. 7. The steel elements were placed along successive rows and columns of nodes in both the longitudinal and transverse directions in a manner that matched, as closely as possible, the amount and location of the actual reinforcement. On the top, a layer of rigid brick elements was added to represent the rigid RC prism monolithically connected to the top of

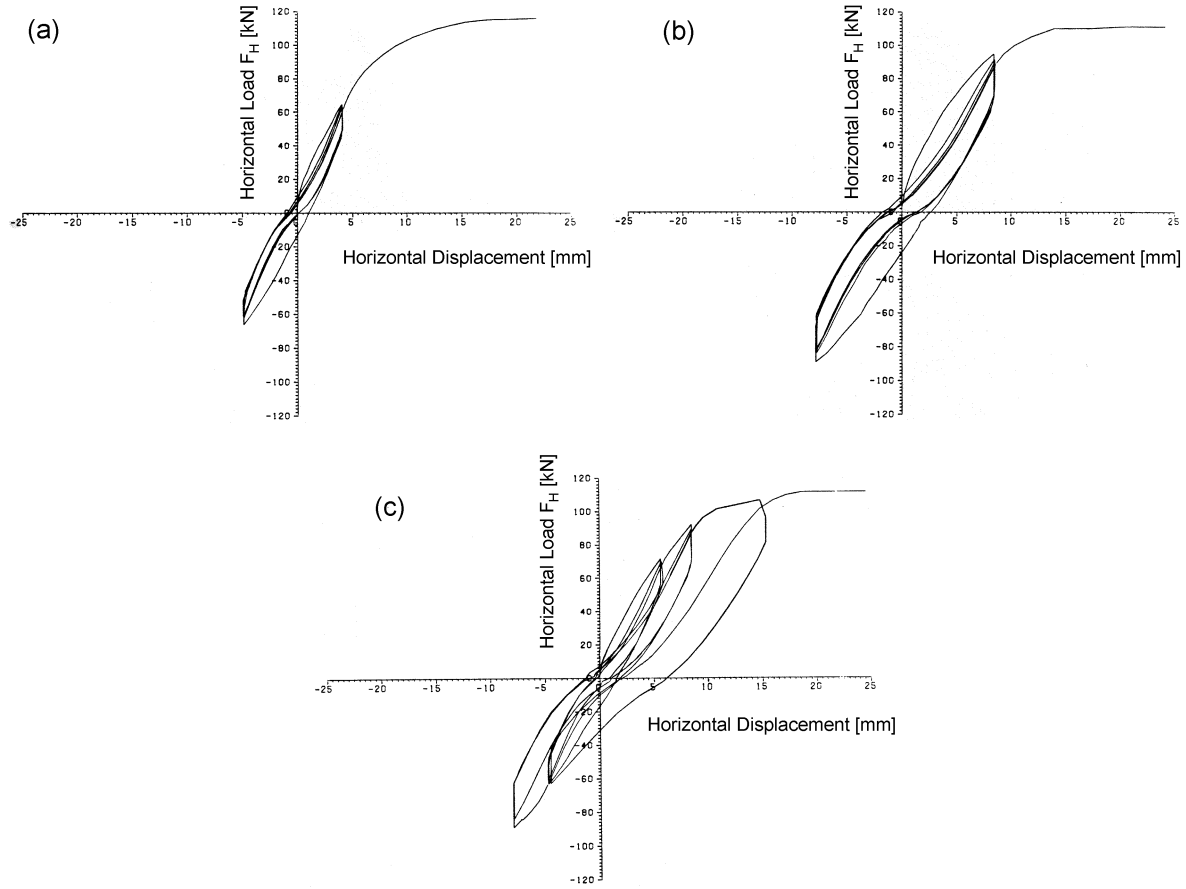

Fig. 6 Experimental response of specimens: (a) SW31, (b) SW32 and (c) SW33

each wall. Because of the symmetry of the specimen's cross-section with respect to the vertical plane in the direction of the applied load, only one half of the actual specimen was modelled. As a result, a smaller number of FE's were used, thus reducing the computational cost. The above symmetry in the FE model was effected by restraining the displacements normal to the plane of symmetry. Finally, the bottom face of the FE mesh was fixed in order to represent the rigid type of foundation imposed in the experiment. It should be noted that, although the experimental load was applied in the form of imposed displacements, in the actual analysis the loads were applied in the form of imposed forces (due to the present capabilities of the existing software). Although this might lead to some deviation of the numerical results from their experimental counterparts at load levels near the wall's load-carrying capacity, such deviation will be minimized by using the smallest possible load increments when applying the external load.

6. Numerical results

Initially, the behaviour of the RC walls is investigated when subjected to monotonic loading

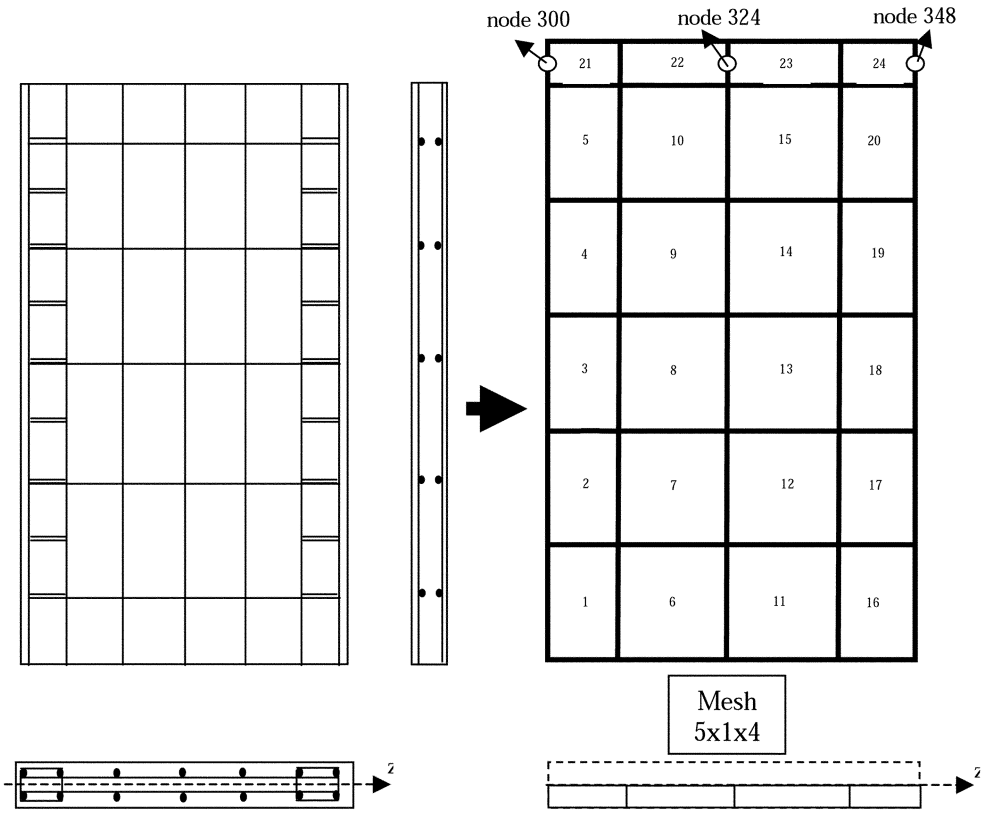

Fig. 7 Structural wall and its FE model

conditions in order to determine numerically their load-carrying capacity, nonlinear behaviour and mode of failure. The load step used so as to avoid instabilities in the numerical procedure was approximately 1/20 of the experimental value of the specimen's load-carrying capacity. The results obtained are presented in Fig. 8 in the form of external load-displacement curves representing the relation between external load and horizontal displacement exhibited by the nodes located at the top element row of the FE mesh. By comparing the horizontal displacement exhibited by three different nodes (i.e. 300, 324 and 348) located at the top element row of the FE mesh (see Fig. 7) it was found that they all exhibit practically the same displacement response. Therefore, the external load-displacement curves used in order to present the numerical results correspond to node 328 throughout.

Typical results describing the cracking processes that specimen SW33 undergoes under monotonic loading are presented in Fig. 9. The cracks begin to appear when the external load becomes 10 kN, and they occur at the bottom left area of the specimen where the tensile stresses are most critical. Gradually, as the imposed load increases, the cracks begin to spread and finally lead to the failure of the specimen. Because all specimens investigated (SW31, SW32 and SW33) are similar (they are not identical since f_c is not the same for all specimens as shown in Table 1) and the loads to which they are subjected are identical, the cracking pattern that develops during loading is practically the same in all three cases. Overall, the numerical results predict that the walls exhibit ductile behaviour

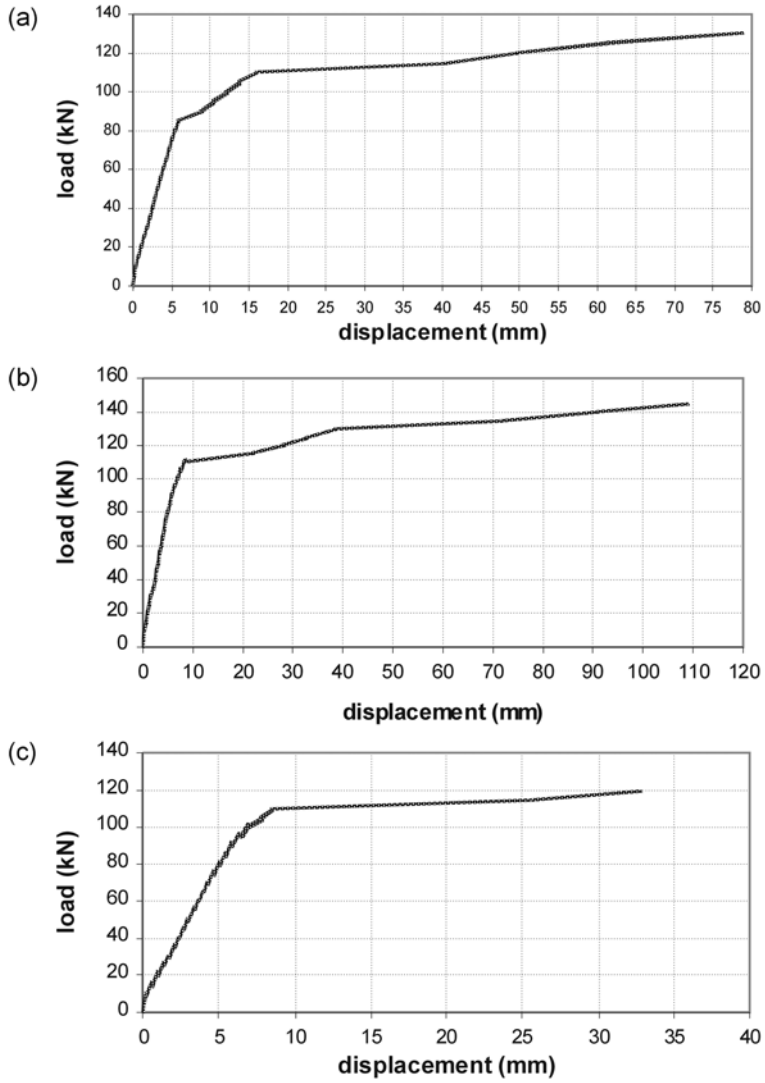

Fig. 8 Load-horizontal displacement curves under monotonic loading for specimens: (a) SW31, (b) SW32 and (c) SW33

since the longitudinal reinforcement yields in tension in the lower region of the wall prior to failure. In doing so, the wall is able to exhibit large displacement under relatively small increments for loads close to is load-carrying capacity.

Following, the monotonic-loading case studies, the specimens were analysed under cyclic loadings equivalent to those imposed in the experimental investigation. The external load is applied in very small force-based load increments (approximately 1/50 to 1/60 of the structure's load-carrying capacity under monotonic loading) in order to avoid numerical instabilities. The choice of load increments smaller than those used in the monotonic case is expected to offer better control over the crack-opening and crack-closure procedures since it will reduce the number of cracks forming and closing during each load step, thus improving the numerical stability of the solution process. The

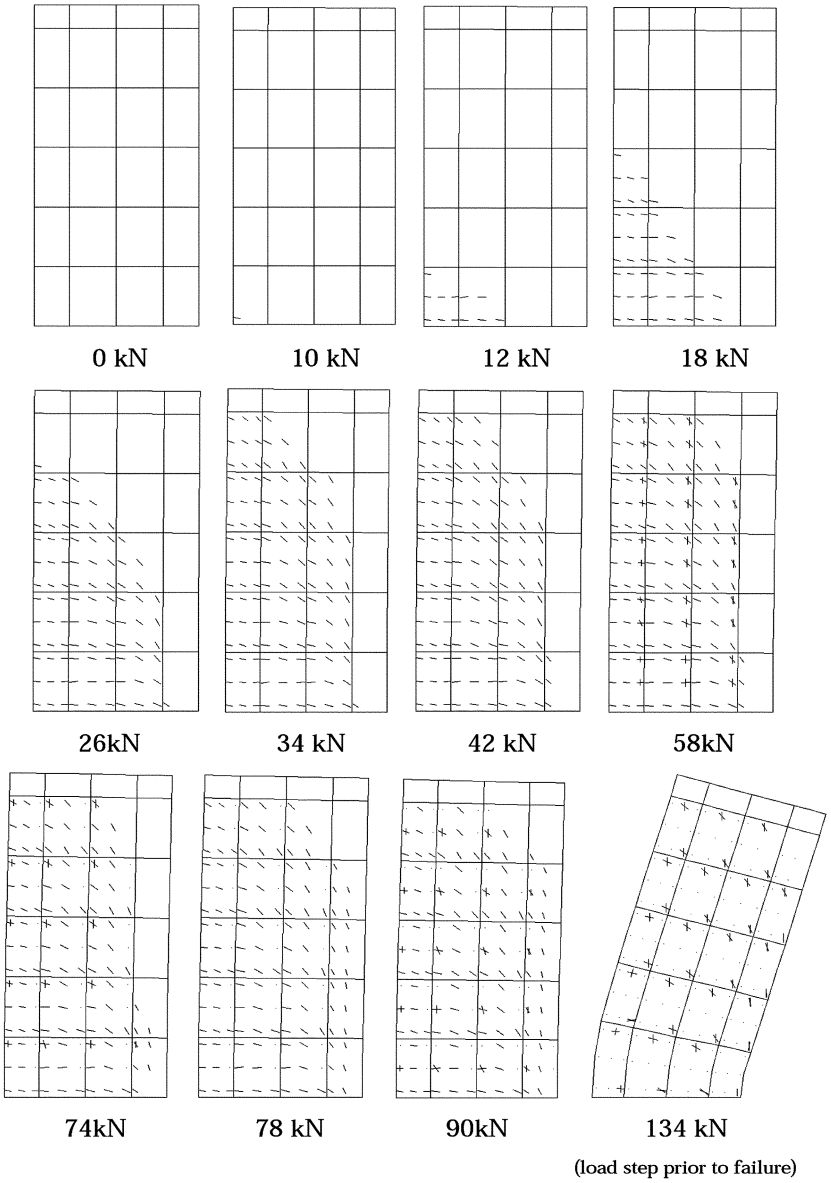

Fig. 9 The development of cracking in specimen SW33 under monotonic loading

results obtained are presented in Figs. 10 to 15 in the form of external load-displacement curves. The curves in Figs. 10, 12 and 14 represent the relation between external load and horizontal displacement at nodes located at the top element row of the FE model. In Figs. 11, 13 and 15 the external load-horizontal displacement curve of each load cycle is presented separately in order to better asses the ability of the program to predict the hysteretic behaviour of the RC walls under different levels of loading.

Typical results describing the cracking process that specimen SW31 undergoes during the first loading cycle are presented in Fig. 16. The cracks begin to appear in the bottom left area of the specimen

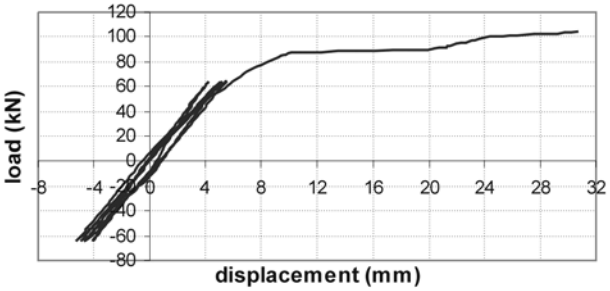

Fig. 10 Load-horizontal displacement curves for specimen SW31

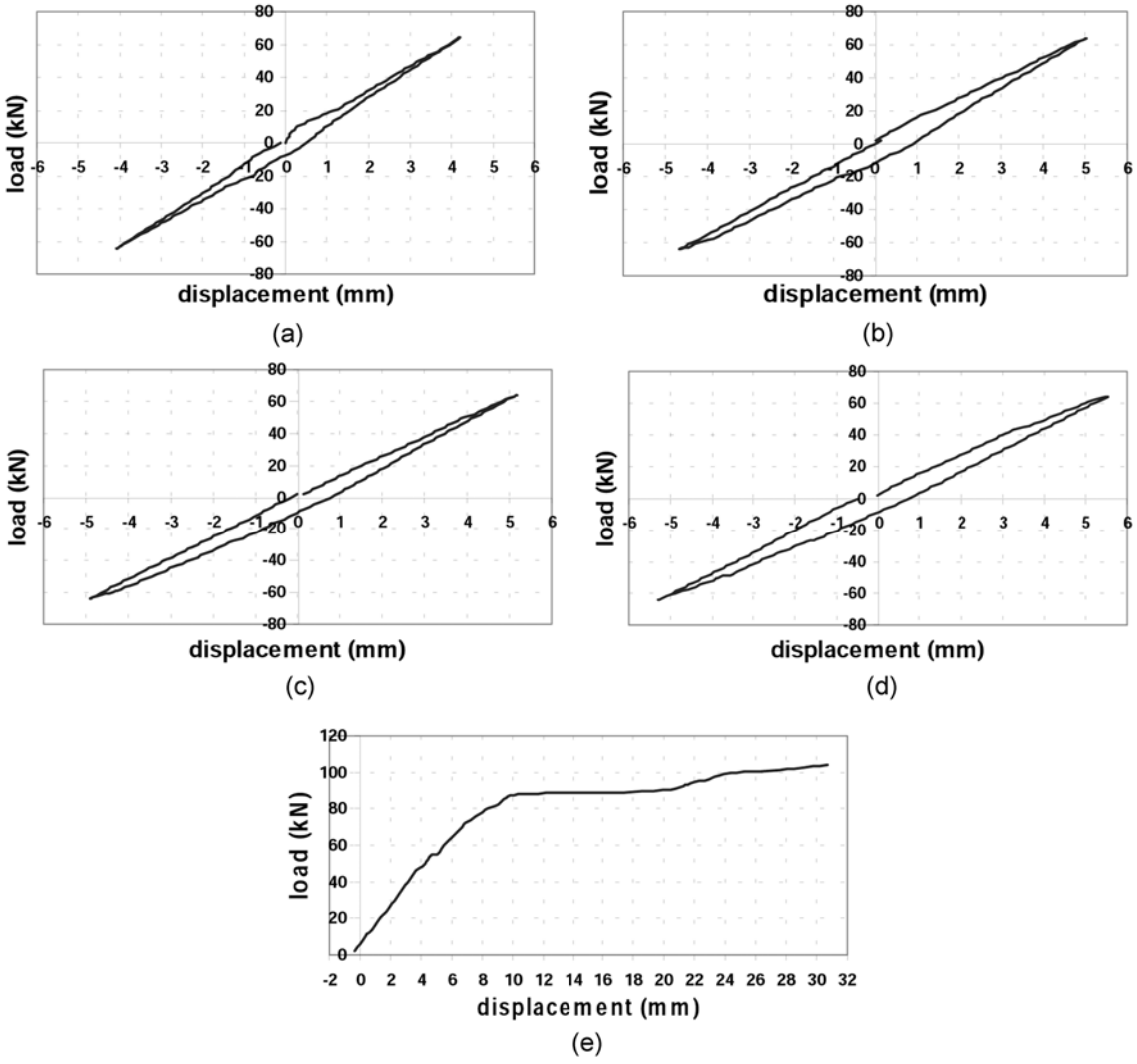

Fig. 11 Load-displacement curves for specimen SW31 for: (a) load cycle 1; (b) load cycle 2; (c) load cycle 3; (d) load cycle 4 (e) final monotonic loading to failure

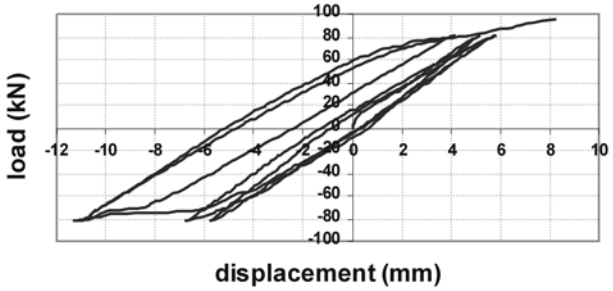

Fig. 12 Load-horizontal displacement curves for specimen SW32

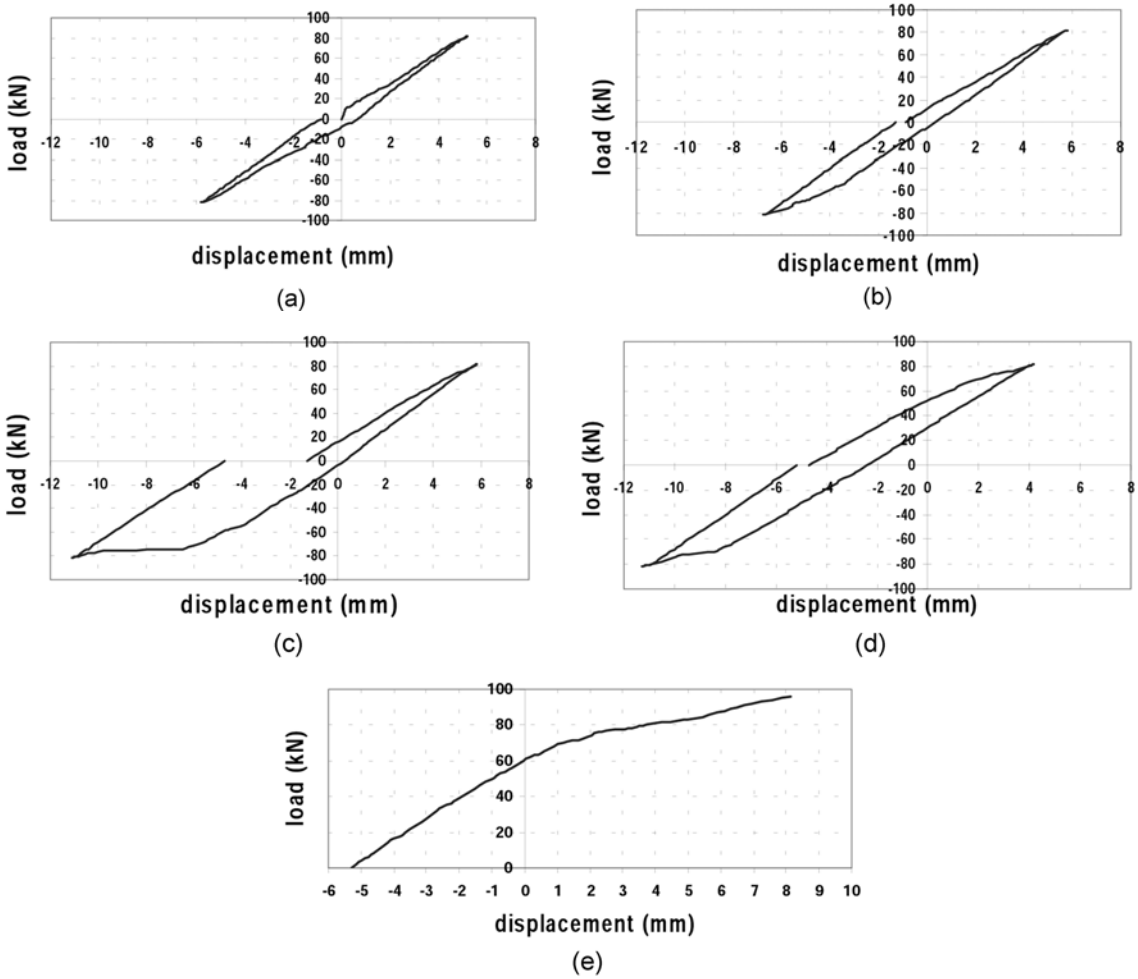

Fig. 13 Load-displacement curves of specimen SW32 for: (a) load cycle 1; (b) load cycle 2; (c) load cycle 3; (d) load cycle 4; (e) final monotonic loading to failure

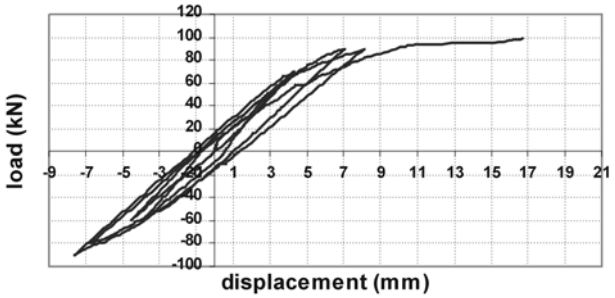

Fig. 14 Load-horizontal displacement curves for specimen SW33

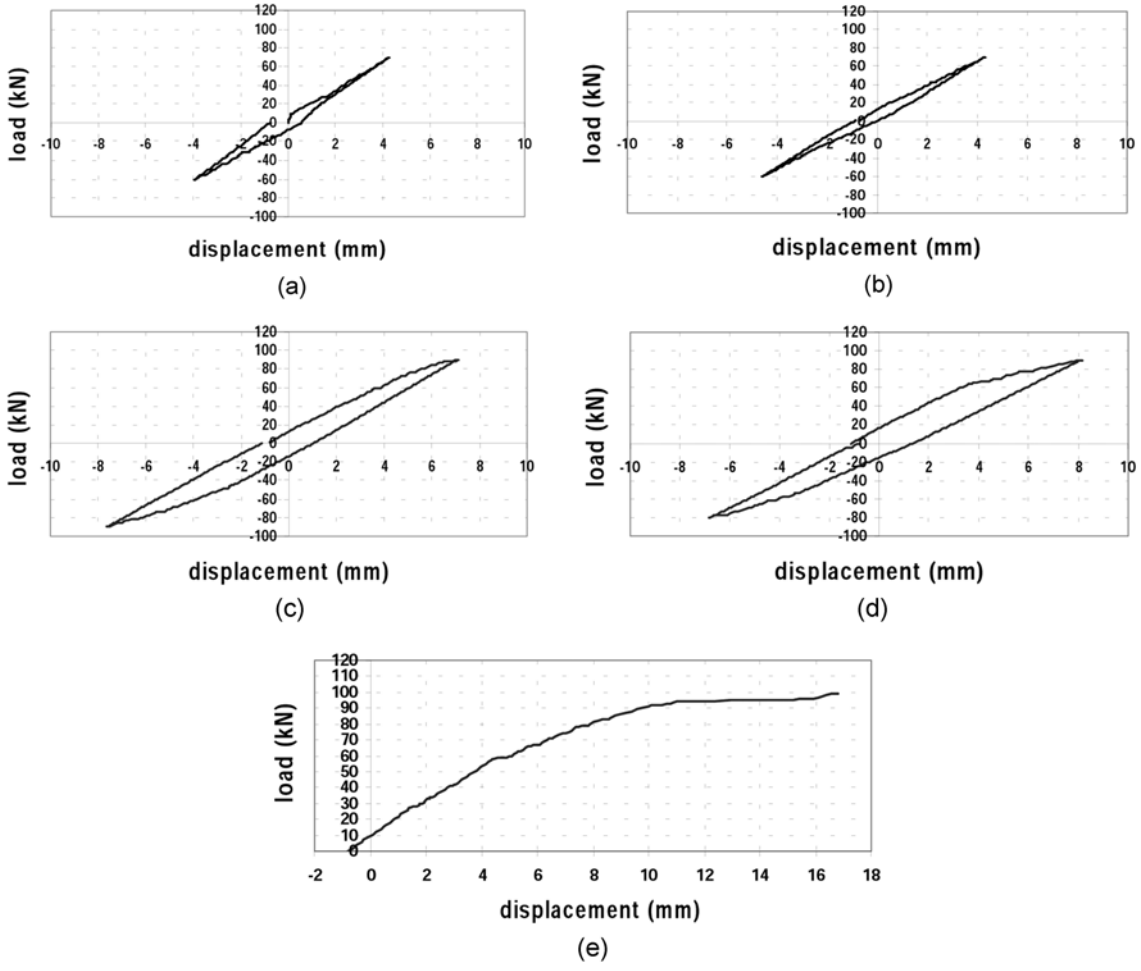

Fig. 15 Load-displacement curves of specimen SW33 for: (a) load cycle 1; (b) load cycle 2; (c) load cycle 3; (d) load cycle 4; (e) load cycle 5 (which was not completed as failure occurred before load reversal)

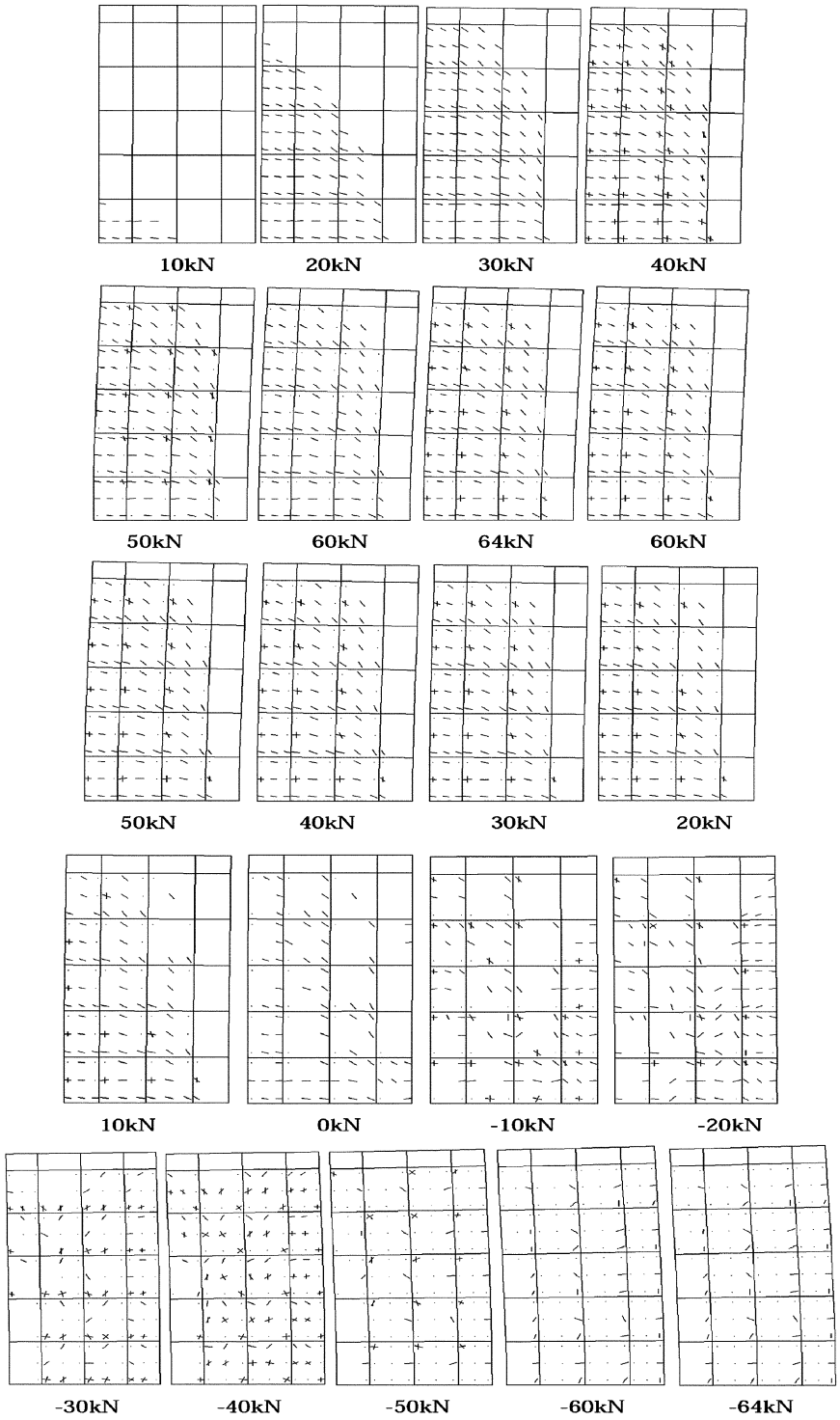

Fig. 16 The development of cracking in specimen SW31 during the first cycle of the cyclic-loading regime

(where the tensile stresses are most critical) at the value of the external load of 10 kN. As the imposed load increases (from 0 to 64 kN), new cracks form. During unloading (from 64 kN to 0 kN) many cracks gradually start to close. When the external load is imposed in the opposite direction (from 0 to -64 kN) the crack-closure procedure continues (although the number of cracks that need to close now are significantly less), but at the same time is followed by the opening of new cracks due to the change in direction of the imposed load.

7. Discussion of numerical results and comparison with experimental data

A comparison between the numerical predictions (cyclic and monotonic case studies) and experimental data for specimen SW31 is presented in Fig. 17. It can be seen that under monotonic loading specimen SW31 had a load-carrying capacity of 130 kN, whereas under cyclic loading its residual load-carrying capacity was found to be 104 kN. It is also evident that the ductility attained under monotonic loading was twice that reached under cyclic-loading conditions. This should mainly be attributed to the fact that the specimen suffered excessive cracking under successive load cycles, thus lowering its ultimate strength and ductility.

The maximum load applied to specimen SW31 at each loading cycle was 64 kN, which is approximately 50% of the (numerically predicted) ultimate strength under monotonic loading and 62% of the (numerically predicted) residual load-carrying capacity when it was loaded to failure after it had been subjected to the prescribed number of loading cycles. At these levels of loading the program did not show any signs of numerical instability during the solution process.

The numerical results obtained from the cyclic-loading case study are similar to the experimental data (this can be seen more clearly in the magnified Fig. 17b), indicating that the program is able to realistically predict the behaviour of RC structures when subjected to this medium level of cyclic loading. The maximum deflection at each load cycle and the corresponding applied load are nearly identical for both data and numerical predictions, the deviation becoming somewhat larger mainly

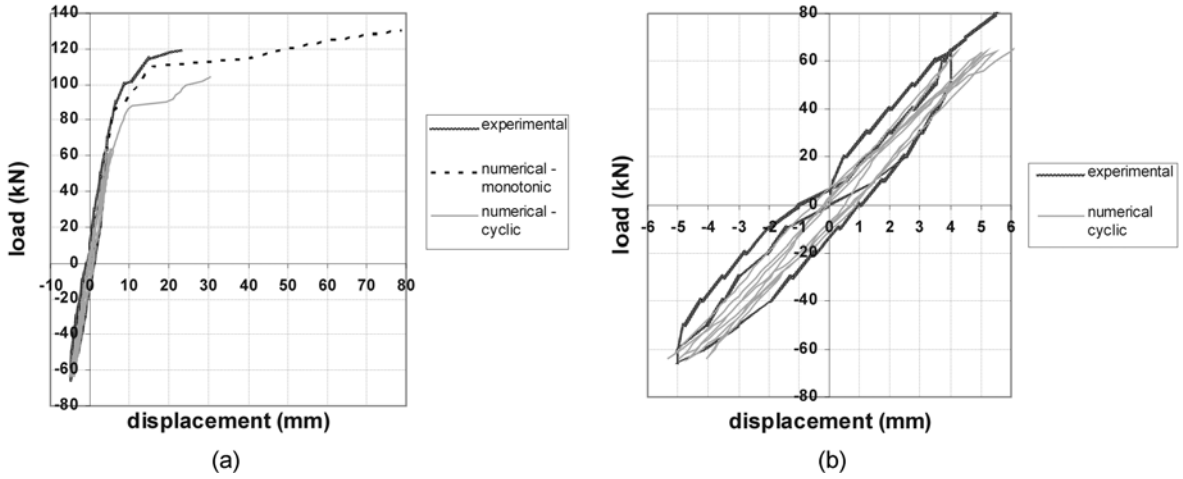

Fig. 17 Comparison between numerical predictions obtained for the monotonic and cyclic case studies with experimental data for specimen SW31: (a) full loading range; (b) region of cyclic loops magnified

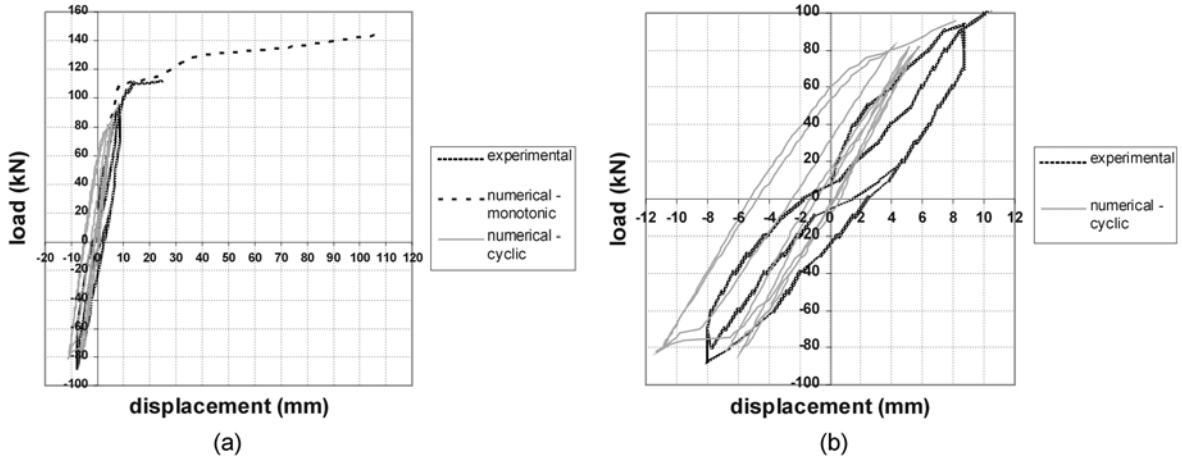

Fig. 18 Comparison between numerical predictions obtained for the monotonic and cyclic case studies with experimental data for specimen SW32: (a) full loading range; (b) region of cyclic loops magnified

when the load was eventually increased monotonically to failure. The experimental results show that specimen SW31 had a load carrying-capacity of 119 kN whereas the numerically predicted load carrying-capacity of the same specimen subjected to the same loading conditions was 104 kN, i.e. 87% of the value of the ultimate strength established experimentally. Similarly good agreement was found for the values of deflections at failure established by experiment (23 mm) and analysis (30 mm). Furthermore, the area enclosed by the hysteretic loops formed by the external load-displacement curves predicted by both experiment and analysis are similar. This area expresses the energy absorbed by the RC wall due to the nonlinear behaviour of concrete due to cracking. The fact that in both cases – experiment and analysis – this area is approximately the same shows that the proposed FE model is able to accurately model the crack opening and closure procedures that the RC wall undergoes during each load cycle.

For the case of specimen SW32 the (numerically) predicted ultimate strength was 145 kN under monotonic loading and 96 kN under cyclic loading (see Fig. 18a). As for the case of specimen SW31, specimen SW32 under cyclic loading failed at a lower load and exhibited smaller maximum deflection when compared to its monotonically-loaded counterpart. The maximum load applied to specimen SW32 at each loading cycle was 84 kN, which is approximately 57% of the specimen's (numerically predicted) ultimate strength when subjected to monotonic loading but 85% of the specimen's (numerically predicted) residual load-carrying capacity when loaded to failure after it had been subjected to the prescribed number of loading cycles. Even at these high levels of loading the program was found to be numerically stable.

By comparing successive cyclic loops of the horizontal load-displacement curve, it appears that the size of these loops increases with the number of cycles. The area of the cyclic loop corresponds to the amount of energy lost due to the nonlinear behaviour of concrete caused by the cracking of concrete and the yielding of steel. The higher cyclic-load level (84 kN) imposed on specimen SW32 appears to have caused more significant cracking and hence a loss of energy larger than that suffered by specimen SW31 which was subjected to a lower level of cyclic load (64 kN).

As for the case of specimen SW31, the numerical results obtained for specimen SW32 under cyclic loading are similar to their experimental counterparts (see Fig. 18), indicating that the

program used is capable of realistically predicting the behaviour of RC structures even when these are subjected to successive levels of loading close to the ultimate strength of the specimen. The maximum deflection at each load cycle and the corresponding load are similar for both experiment and analysis. Furthermore, as in the case of SW31, the area enclosed by the hysteretic loops formed by the external load-displacement curves predicted by both experiment and analysis are similar, thus proving once again that the FE model adopted in the current investigation is efficient in modelling the cracking procedure that concrete undergoes. Under cyclic loading, the experimental results indicate that specimen SW32 had a load-carrying capacity of 112 kN, whereas the numerically predicted load-carrying capacity of the specimen under the same loading conditions was 96 kN or approximately 86% of the ultimate strength established experimentally.

However, a discrepancy in the maximum attained deflection is noticeable in the last stage when the load increased monotonically to failure. Experimentally, this maximum deflection was recorded to be around 20-25 mm, whereas the numerical prediction is 9 mm. The main reason for such differences is the fact that in the numerical investigation failure is considered to occur when the structure's stiffness matrix becomes non-positive definite whereas in the actual experiment failure occurs when the RC structural form under investigation suffers total loss of its load-carrying capacity. In the present case, this occurred due to the disruption of the continuity of concrete caused by excessive crack formation in the lower area of the RC wall. After the degradation of the concrete within the lower regions of the wall, the actual structure used in the test may still have been capable of maintaining its load-carrying capacity through alternative resistance mechanisms such as, for example, dowel action. However, this type of behaviour cannot be described analytically, as the development of such alternative resistance mechanisms are not allowed for by the analysis procedure developed and used in the present work. It is significant to note that, when observing the experimental results, it is clear that in the final stages of the loading procedure the external load-displacement curve becomes practically horizontal beyond a displacement of about 13 mm (comparable with the numerical prediction of 9 mm) which mean thats, at this point, the RC wall has suffered extensive cracking (especially in its lower area) which has led its stiffness to drop dramatically and that the RC wall is resorting to alternative resistance mechanisms. Evidently, such alternative

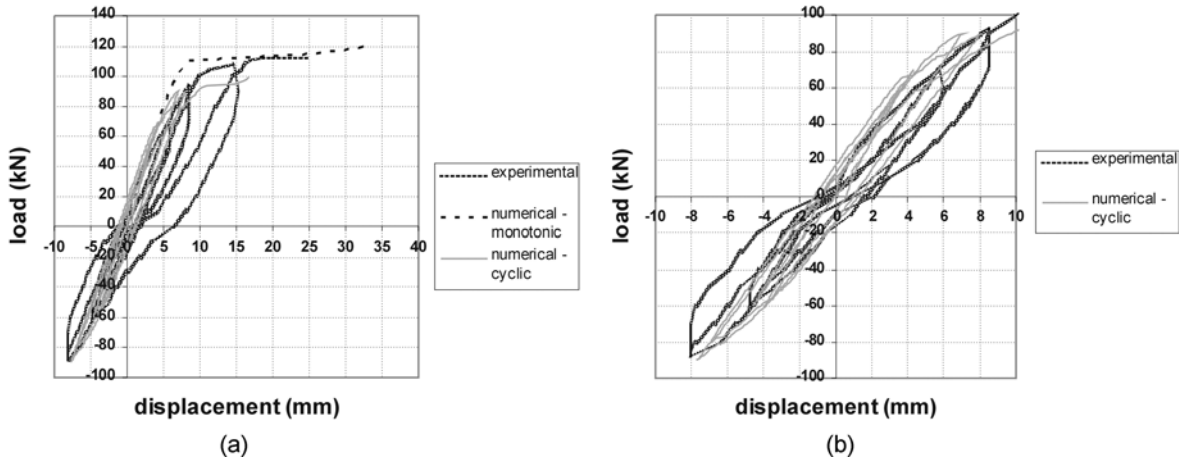

Fig. 19 Comparison between numerical predictions obtained for the monotonic and cyclic case studies with experimental data for specimen SW33: (a) full loading range; (b) region of cyclic loops magnified

mechanisms (not catered for by the numerical model) are highly unstable, of short duration, and cannot be relied upon in safe design: they are really manifestations of post-failure phenomena and, as such, are of no relevance to designers.

In the last case study, the ultimate strength of specimen SW33 predicted by the program was 120 kN when subjected to monotonic loading but, under cyclic loading, the program was unable to complete all the prescribed loading cycles: namely, in the experiment there had been 5 cycles followed by monotonic loading to failure, while in the FE analysis failure occurred during the 5th load cycle due to premature failure of the specimen during the 5th load cycle (Fig. 19). The maximum load applied to specimen SW33 at the two initial loading cycles was 64 kN whereas for the next two it was 90 kN. After concluding these loading cycles the specimen failed at the last prescribed loading cycle at a load level of 100 kN which is close to the specimen's (experimentally determined) load-carrying capacity (112 kN).

The experimental maximum deflection at each load cycle and the corresponding applied load are similar to the deflections predicted by the program and the corresponding imposed load (see Fig. 19). The maximum load applied to specimen SW33 during the first two loading cycles was 70 kN, which is approximately 53% of the (numerically predicted) ultimate strength under monotonic loading and 70% of the (numerically predicted) residual load-carrying capacity when it was loaded to failure after it had been subjected to the prescribed number of loading cycles. Then, the maximum load applied to specimen SW33 during loading cycles 3 and 4 was increased to 90 kN, which is approximately 75% of the (numerically predicted) ultimate strength under monotonic loading and 90% of the (numerically predicted) residual load-carrying capacity in the cyclic case study. At these levels of loading the FE scheme did not show signs of numerical instability during the solution process, proving again that the program used is capable of realistically predicting the behaviour of RC structures when subjected to levels of cyclic loading close to the ultimate strength of the specimen.

The experimental results indicate that specimen SW33 had a load-carrying capacity of around 112 kN, whereas the numerically predicted load-carrying capacity of the specimen under the same loading conditions was 100 kN, or approximately 89% of the ultimate strength established experimentally. Furthermore, the maximum deflection established experimentally was found to be about 25 mm whereas in the numerical investigation it was found to be 17 mm. Moreover, as in the case of SW31 and SW32, the area enclosed by the hysteretic loops formed by the external load-displacement curves predicted by both experiment and analysis are similar, thus proving that the FE model adopted in the current investigation is efficient in modelling the cracking procedure that concrete undergoes even during load cycles in which the level of external loading reaches the load-carrying capacity of the specimen.

The premature failure of the specimen (in terms of the number of cycles attained, namely four and a half instead of five and a half) of the specimen in the last load cycle and the small deviation between experimental and numerical predictions could be attributed to the fact that, as in case of RC wall SW32, failure, during the numerical investigation, is considered to occur when the structure's stiffness matrix becomes non-positive definite and that at this stage the RC structure is resorting to alternative resistance mechanisms such as, for example, dowel action, in order to extend (albeit very briefly) its load carrying-capacity.

8. Some observations on the material model used and their implications for structural design

The material model adopted herein has been outlined in detail in books on analysis (Kotsovos and Pavlović 1995) and design (Kotsovos and Pavlović 1999) of structural concrete. Nevertheless, some of the ensuing material features and their implications in plain, reinforced and prestressed concrete structures are presented here, especially for those readers not familiar with the book.

First, it should be stressed that the material model is applicable to all structural concrete forms, irrespective of their mode of failure. Thus, more than a hundred problems have been presented encompassing plain, reinforced and prestressed concrete members/structures, and the material model was found to provide good predictions in all cases, and independently of the failure mode (flexural/ductile, shear/brittle). Thus, although the structural walls analysed in this paper failed in flexure, there is no reason to suggest that the present FE model would not give accurate predictions of "shear" failures. Of course, most of the available test data refer to what one might term "good design practice" (flexural or ductile behaviour), and it is difficult to find data on "undesirable designs" involving shear or brittle failure. This is the reason why the latter have not been included herein (admittedly, such poor designs are unlikely to survive more than one cycle of loading unless the loading amplitude is very low).

Secondly, the brittle nature of the material model does not imply a "no-tension" material since test data (uniaxial, biaxial and triaxial) on concrete cylinders under definable conditions have produced failure envelopes in both compression and tension (or combinations of these in the three-dimensional stress space). Thus, unreinforced (plain) concrete structures can exhibit finite (and, often, considerable) load-carrying capabilities, especially in the case of structural forms amenable to stress redistribution in the course of ongoing cracking.

Thirdly, the undeniable triaxial behaviour of concrete just prior to local (material) failure produces, invariably, tensile – never compressive – failures (in the sense that at least one of the three principle stress counterparts must be tensile): ample evidence for this is contained in the work of Kotsovos and Pavlović (1995) where the physical basis for the sheer incompatibility between triaxiality and purely compressive failure is clearly explained (pp 103-125). Such a view is confirmed by the fact that, although pure compressive material failure is allowed for in the FE program, no FE run (irrespective of problem type) has, to date, recorded such an instance anywhere within the member/structure. What is usually believed to be the "crushing" of concrete in flexural failures is a post-failure phenomenon, namely it is the effect but not its cause: such flexural failures are invariably initiated by a tensile crack in the compressive region (again, failure is associated with the least one principal-stress component) after which the thin column of concrete becomes detached from the rest of the member and then immediately buckles due to the very large compression which this thin column (as opposed to the three-dimensional continuum) can no longer sustain – this is clearly illustrated by a typical beam example (Kotsovos and Pavlović 1995) where the experimental photograph of the tested beam (pp 431) and the crack pattern predicted by the FE program (pp 435) are in obvious agreement.

9. Conclusions

Through the comparative study between the numerical predictions and the experimental data, it is

established that the nonlinear strategy adopted is able to describe the hysteretic behaviour of concrete even when the RC specimens are subjected to high levels of loading, i.e., close to their load-carrying capacity. Any deviation between experimental results and numerical predictions are within the order of accuracy of structural engineering design and are due to a number of causes. These include post-failure phenomena, applied load control instead of displacement control (especially relevant when large increases in displacement under constant load are experienced, as in the case of specimen SW32), and even time-dependent effects (Lefas 1988). The latter, however, are more noticeable in static cyclic tests (as those presently modelled) where cracking in the concrete medium continues to evolve even when the external load remains constant (such effects becoming more apparent as the value of the applied load increases and approaches the load-carrying capacity of the specimen), whereas these effects are less prominent in dynamic analysis.

It may be concluded, therefore, that, despite the small divergence between experimental and numerical results, the nonlinear procedure adopted in the FE model used in the present work was found to perform satisfactorily, providing a realistic description of the hysteretic behaviour of RC structural elements under cyclic loading even when this was of a severe and static nature. The use of this model to describe the behaviour of RC structures under dynamic cyclic loading (Cotsovos 2004) has yielded equally satisfactory results, as will be reported in future publications.

Acknowledgements

The authors wish to thank one of the reviewers for his helpful comments which prompted the additional explanatory penultimate section of the paper.

References

Al-Gadhib, A. H., Asad-ur-Rahman, K. and Baluch, M. H. (1998), "CDM based finite element code for concrete in 3-D", *Computers & Struct.*, **67**, 451-462.

Al-Gadhib, A. H., Baluch, M. H., Shaalan, A., Khan, A. R. (2000), "Damage model for monotonic and fatigue response of high strength concrete", *Int. J. Damage Mech.*, **9**, 57-78.

Baluch, M. H., Al-Gadhib, A. H., Khan, A. R. and Shaalan, A. (2003), "CDM model for residual strength of concrete under cyclic compression", *Cement & Concrete Composites*, **25**, 503-512.

Cela, J. J. L. (1998), "Analysis of reinforced concrete structures subjected to dynamic loads with a viscoplastic Drucker-Prager model", *Appl. Math. Modelling*, **22**, 495-515.

Chen, W.-F. (1988), *Plasticity for Structural Engineers*, New York, Springer.

Chen, E.-S. and Buyukozturk, O. (1985), "Constitutive model for concrete in cyclic compression". *J. Eng. Mech. Div.*, ASCE, **111**, 797-815.

Chen, A. C. T. and Chen, W.-F. (1975), "Constitutive relations for concrete", *J. Eng. Mech. Div.*, ASCE, **101**, 465-481.

Cotsovos, D. M. (2004), "Numerical Modelling of Structural Concrete under Dynamic Loading (Earthquake and Impact)", PhD thesis, University of London.

Dube, J.-F., Pijaudier-Cabot, G. and La Borderie, C. (1996), "Rate dependent damage model for concrete in dynamics", *J. Eng. Mech. Div.*, ASCE, **122**, 359-380.

Faria, R., Olivera, J. and Cevera, M. (1998), "A strain-based plastic viscous-damage model for massive concrete structures", *Int. J. Solids. Struct.*, **35**, 1533-1558.

Fardis, M. N., Alibe, B. and Tassoulas, J. L. (1983), "Monotonic and cyclic constitutive law for concrete", *J. Eng. Mech. Div.*, ASCE, **109**, 516-536.

Grassl, P., Lundgren, K. and Gylltoft, K. (2001), "Concrete in compression: A plasticity theory with a novel hardening law", *Int. J. Solids Struct.*, **39**, 5205-5223.
Hatzigeorgiou, G., Beskos, D., Theodorakopoulos, D. and Sfakianakis, M. (2001), "A simple concrete damage model for dynamic FEM applications", *Int. J. Computational Eng. Sci.*, **2**, 267-286.
Kang, H. D., William, K., Shing, B. and Spacone, E. (2000), "Failure analysis of RC columns using a triaxial concrete model", *Computers & Struct.*, **77**, 423-440.
Kotsovos, M. D. (1979), "Effect of stress path on the behaviour of concrete under triaxial stress states", *ACI J.*, **76**, 213-223.
Kotsovos, M. D. (1983), "Effect of testing techniques on the post-ultimate behaviour of concrete in compression", *Materials & Struct.*, *RILEM*, **16**, 3-12.
Kotsovos, M. D. and Pavlović, M. N. (1995), *Structural Concrete: Finite-element analysis and design*, London, Thomas Telford.
Kotsovos, M. D. and Pavlović, M. N. (1999), *Ultimate limit-state design of concrete structures: a new approach*, London, Thomas Telford.
Kotsovos, M. D. and Spiliopoulos, K. V. (1998), "Modelling of crack closure for finite-element analysis of structural concrete", *Computers & Struct.*, **69**, 383-398.
Kwak, H.-G. and Kim, D.-Y. (2004), "Cracking behavior of RC shear panels subjected to cyclic loadings", *Computers & Concrete*, **1**, 77-98.
Lefas, I. (1988), "Behaviour of reinforced concrete walls and its implementation for ultimate limit state design", *Ph.D. J. Thesis*, University of London.
Mazars, J. (1986), "A description of micro and macroscale damage of concrete structures", *Eng. Fracture Mech.*, **25**, 729-737.
Murray, D. W., Chitnuyanondh, L., Rijub-Agha, K. Y. and Wong, C. (1979), "Concrete plasticity theory for biaxial stress analysis", *J. Eng. Mech. Div.*, ASCE, **105**, 989-1005.
Papa, E. and Taliercio, A. (1996), "Anisotropic damage model for the multiaxial static behaviour of plain concrete", *Eng. Fracture Mech.*, **55**, 163-179.
Winnicki, A. and Cichon, C. (1998), "Plastic model for concrete in plain stress state. I: Theory", *J. Eng. Mech.*, **124**, 591-602.
Winnicki, A. and Cichon, C. (1998), "Plastic model for concrete in plain stress state. II: Numerical validation", *J. Eng. Mech.*, **124**, 603-613.
Winnicki, A., Pearce, C. J. and Bicanić, N. (2001), "Viscoplasic Hoffman consistency model for concrete", *Computers & Struct.*, **79**, 7-19.
Yang, B.-L., Dafalias, Y. F. and Herrmann, L. R. (1985). "A bounding surface plasticity model for concrete", *J. Eng. Mech. Div.*, ASCE, **111**, 359-380.
Yasuhiro, C. O. and Chen, W.-F. (1987). "Hypoplastic-perfectly plastic model for concrete materials", *J. Eng. Mech. Div.*, ASCE, **113**, 1840-1860.
Van Mier, J. G. M (1984), "Strain-softening of concrete under multiaxial loading conditions", PhD thesis, Eindhoven University of Technology.
Van Mier, J. G. M, Shah, S. P., Armand, M., Balayssac, J. P., Bascoul, A., Choi S., Dasenbrock, D., Ferrara, G., French, C., Gobbi, M. E., Karihaloo, B. L., Konig, G., Kotsovos, M. D., Labuz, J., Lange-Korbar, D., Markeset, G., Pavlović, M. N., Simsch, G., Thienel, K-C, Turatsinze, A., Ulmer, M., van Geel, H. J. G. M., van Vliet, M. R. A. and Zissopoulos, D. (1997), "Strain softening of concrete in uniaxial compression", *Materials and Structures*, *RILEM*, **30**, 195-209.
Zissopoulos, P. M., Kotsovos, M. D. and Pavlović, M. N. (2000) "Deformational behaviour of concrete specimens in uniaxial compression under different boundary conditions", *Cement and Concrete Res.*, **30**, 153-159.

CC